Research Article

Flow in a two dimensional channel with deforming and peristaltically moving walls

Roohi Laila[1] · Dil Nawaz Khan Marwat[1] · Kamran Khan[1] · Aamir Ali[2] · Zahir Shah[3,4]

Received: 16 September 2019 / Accepted: 20 October 2019 / Published online: 4 November 2019

Abstract
In this paper, effects of deforming walls on peristaltic flow in a two dimensional channel have been investigated. The two dimensional form of the governing equations is simplified by using appropriate transformations and well established approximations, which are used extensively for solution of such models. The transformations are designed so that the complex problem is reduced into an ordinary differential equation (ODE). New and simple non-linear ODE is formed in view of adopted procedures and techniques. Its solutions are exactly matched with the solutions of classical problems. Solutions of the final problem are provided for small values of the surface expansion (contraction) ratio and Reynolds number with the help of the perturbation technique and non-linear shooting method. The velocity field, pressure and shear stress are evaluated analytically and numerically. Meanwhile, effects of all parameters are observed on the velocity field, pressure rise per wavelength and shear stress profiles with the help of tables and different figures. Excellent agreement between solutions is found. Current results are apparently matched with the classical problems of peristaltic flow in deforming and non-deforming walls.

Keywords Surface deformation · Peristaltic pumping

1 Introduction

Peristalsis is the mechanism of fluid transport through elastic channels, chambers and pipes by means of sinusoidal waves. There are many agents that are producing fluid motion in which some sources are very active and prominent. For example pressure gradients and surface (solid body, wall and plate) motion (deformation, peristaltic motion) may cause fluid motion. The phenomenon of peristalsis has many applications in biology and engineering. In many physiological systems, the peristaltic motion of different body parts are producing fluid transportation. The ureter's muscles undergo repeated contraction (expansion) together with peristaltic movement and thoroughly pump urine from kidney into the bladder and similarly the spermatozoa moves in this way in ducts. On the other hand, the contraction and relaxation of muscles combined with peristaltic motion is also responsible for digestion of food. Besides these, it is widely used in manipulating the biomedical devices and machines, house pumps, finger and roller pumps that are used to force blood and other fluids. Due to its numerous applications, the phenomenon has attracted many scientists, engineers, mathematicians and tremendous research have been carried out on peristaltic pumping [1–17].

✉ Aamir Ali, aamir_ali@cuiatk.edu.pk | [1]Department of Mathematics, Faculty of Technology and Engineering Sciences, Islamia College Peshawar, Jamrod Road, University Campus, Peshawar, Khyber Pakhtunkhwa 25120, Pakistan. [2]Department of Mathematics, COMSATS University Islamabad, Attock Campus, Kamra Road, Attock 43600, Pakistan. [3]Center of Excellence in Theoretical and Computational Science (TaCS-CoE), SCL 802 Fixed Point Laboratory, Science Laboratory Building, King Mongkut's University of Technology Thonburi (KMUTT), 126 Pracha-Uthit Road, Bang Mod, Thrung Khru, Bangkok 10140, Thailand. [4]KMUTT-Fixed Point Research Laboratory, Room SCL 802 Fixed Point Laboratory, Science Laboratory Building, Department of Mathematics, Faculty of Science, King Mongkut's University of Technology Thonburi (KMUTT), 126 Pracha-Uthit Road, Bang Mod, Thrung Khru, Bangkok 10140, Thailand.

SN Applied Sciences (2019) 1:1534 | https://doi.org/10.1007/s42452-019-1547-4

The first attempt is made by Shapiro [1] and he solved the peristaltic flow problem for a two dimensional tube with assumptions of small Reynolds number and long wave length. He assumed a peristaltic wave of very long wave length and the aspect ratio of wave length to the diameter of tube is greater than four. The closed form solutions of Shapiro for the modeled equations are very famous and obviously reduced it to well-known Poiseuille solutions. The problem of peristaltic flow is further analyzed by assuming the sinusoidal waves [6] and arbitrary shapes waves [7]. The theoretical data is experimentally verified in [8] and latest techniques and methods are provided. These analysis are propitious to the fundamental concepts which can help us in analyzing the problems and provide solutions to a new hydrodynamic systems. The peristaltic flow problem for two dimensional channel is solved numerically see [9, 10] and found excellent agreement between the experimental and theoretical inquiries.

A lot of research articles are appeared in the literature witch presents the flow between deforming and porous walls [11–15]. Majdalani [12] extended the scope of deformable channels flow and used similarity variables for the solution of model problem. Matebese [16] studied the flow model of a deformable channel where the gap between walls in filled with porous medium and assumed a variable magnetic field. A more complex model is studied by Khan Marwat and Asghar [17] and they investigated the coupled effects of wall contraction (expansion) and peristalsis in a deformable channel and recovered the solutions of [1] for zero wall deformation ratio (α). A lot of research work are available for static and moving walls for both Newtonin, non-Newtonin and Jeffery fluids in nano or in micropolar fluid, see [18–23]. Akram et al. [18] analyzed the Peristaltic pumping of a Jeffrey fluid with double-diffusive convection in nanofluids in the presence of inclined magnetic field. Sadaf et al. [19] and Shehzadi and Nadeem [20] discussed the fluid flow between walls for peristaltic transportation in a chanel. Sadaf et al. [19] discuss this phenominan for Nano fluid with MHD effects while Shehzadi and Nadeem [20] consider a porous medium with porous boundary conditions for this study with out MHD effects.

For the best of auther's informations, we include some other slassical work in this section which are discussed by [24, 25]. Saleem et al. [24] modeled the problem associated with fow, heat, and mass transfer features of gyrotactic microorganisms containing MHD Jefrey fuid over a vertical cone with nanoparticles. Qasim et al. [25] examined the effects of nonlinear thermal radiation on the flow of Jeffrey fluid over a radially stretching sheet with variable thermal conductivity.

Here we present a model of fluid flow between peristaltically moving and deforming walls. More precisely, we study the consequences of deformable surfaces on peristaltic flow in a two dimensional channel. Note that the channel is contracting (expanding) with time. A set of transformations is introduced such that the generalized wall's geometry is invoked in the new variables. In view of these new variables, the governing equations are converted into the simplest PDE's. Later on, the wall geometry is specified and modified by the well-known peristaltic and deforming walls shapes. Besides that, the assumptions and approximation of long wavelength and small deformation ratio are employed so that the governing PDE's are converted into an ODE. The ODE is new, simple and gives the results of [17] for fixed and special value of the parameters. Perturbation and numerical methods are used for the solution of modeled problem. The flow field properties have been evaluated by numerical means and new results are found for velocity components, pressure and shear stress. The profiles of velocity field, pressure rise per wavelength and shear stress are discussed in detail for different values of Reynolds number and wall deformation ratio. Note that the behavior of all these quantities is recorded in different tables. The two different solutions are compared in tables and graphs. The ranges of parameters are so chosen for which error between the solutions is very negligible. New results are also matched with [17] and further analysis of the transformation in hand, may give rise to new research problems. The advantage and usefulness of the transformation and approximation is very clear and obviously converts the complex problem into a simplest one. The last problem is easy to solve and provides accurate and authentic results.

2 Mathematical formulation

We have taken two parallel plates and the gap between walls is filled with viscous fluid such that the vertical distance between walls in $2h(x,t)$ where x represents the horizontal axis, lie along the channel and t is time variable. Note that y in normal to x-axis in vertical direction. Further, it is assumed that the flow is two dimensional, therefore, the velocity vector has two component i.e.$u = u(x,y,t)$ and $v = v(x,y,t)$ which lies along x and y directions, respectively. A sinusoidal waves are generated at walls with speed c in the axial direction, whereas the space between upper and lower walls changes with time. In other words, the walls of the channels are contracting and expanding in time t. The flow geometry is given in Fig. 1, however, the upper wall is presented by the following mathematical form:

$$h(x,t) = a(t) + bsin(\gamma) \tag{1}$$

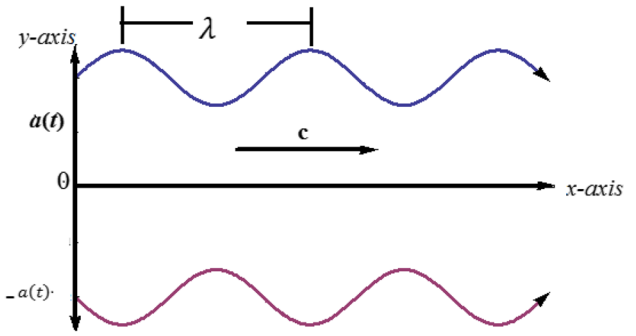

Fig. 1 Flow geometry and channel under consideration

in which $\gamma = \frac{2\pi}{\lambda}(x - ct)$, such that the wave amplitude (b), wavelength (λ) and wave speed (c) are the known quantities in the above relation.

A deformable channel means that the parallel walls are contracting and expending in y-direction only. Note that the distance between walls is changing with space (x) and time (t). The two dimensional flow problem is presented in mathematical terms by considering the continuity and Navier–Stokes equations. In addition, the body forces have no role in flow region and finally the governing equation are reduced to the following form:

$$\frac{\partial u}{\partial x} + \frac{\partial v}{\partial y} = 0, \tag{2}$$

$$\frac{\partial u}{\partial t} + u\frac{\partial u}{\partial x} + v\frac{\partial u}{\partial y} = -\frac{1}{\rho}\frac{\partial p}{\partial x} + \upsilon\left[\frac{\partial^2 u}{\partial x^2} + \frac{\partial^2 u}{\partial y^2}\right], \tag{3}$$

$$\frac{\partial v}{\partial t} + u\frac{\partial v}{\partial x} + v\frac{\partial v}{\partial y} = -\frac{1}{\rho}\frac{\partial p}{\partial y} + \upsilon\left[\frac{\partial^2 v}{\partial x^2} + \frac{\partial^2 v}{\partial y^2}\right] \tag{4}$$

In which the pressure (p), density (ρ), kinematic viscosity $\left(\upsilon = \frac{\mu}{\rho}\right)$ and absolute viscosity (μ) are fluid thermophysical properties which describe the fluids behavior. The thermal properties are assumed to be constant. The governing Eqs. (2)–(4) are simplified with the help of transformations and new set of variables is introduced i.e. $\chi = \chi(x,t), \quad \eta = \eta(x,y.t)$ where $\eta = \frac{y+h}{2h}$ and $\chi = \alpha\ln(h) + \beta(t)$, so that Eq. (2) is reduced to the following form:

$$2\alpha h_x\frac{\partial u_1}{\partial \chi} + 2h_x\left(\frac{1}{2} - \eta\right)\frac{\partial u_1}{\partial \eta} + \frac{\partial v_1}{\partial \eta} = 0. \tag{5}$$

Note that u_1 and v_1 are defined in Eq. (6). The continuity equation is eliminated by introducing the steam function (ψ_1) and the velocity components are defined such that $u = \frac{\partial \psi_1}{\partial y}, v = -\frac{\partial \psi_1}{\partial x}$. In view of the dimensionless stream function $\psi = \frac{\psi_1}{\upsilon}$, the velocity components, defined in the above relations are transformed as:

$$\begin{aligned} u_1(\chi,\eta,t) &= \frac{\upsilon}{2h}\psi_\eta + c, \\ v_1(\chi,\eta,t) &= -\frac{\upsilon h_x}{h}\left[\alpha\psi_\chi + \left(\frac{1}{2} - \eta\right)\psi_\eta\right] \end{aligned} \tag{6}$$

where the subscripts are representing the partial derivatives w.r.t. indicated variables. The well-known vorticity equation is formed by eliminating pressure terms between Eqs. (3) and (4)

$$\frac{\partial \xi_1}{\partial t} + u\frac{\partial \xi_1}{\partial x} + v\frac{\partial \xi_1}{\partial y} = \upsilon\nabla^2\xi_1 \tag{7}$$

where $\xi_1 = \frac{\partial v}{\partial x} - \frac{\partial u}{\partial y} = -\nabla^2\psi_1, \nabla^2 = \frac{\partial^2}{\partial x^2} + \frac{\partial^2}{\partial y^2}$. Inserting the expressions for u_1 and v_1 from Eq. (6) into the vorticity function, we obtained that:

$$\begin{aligned} -\xi_1 = {} & \upsilon\alpha H'\psi_\chi + \alpha^2\upsilon H^2\psi_{\chi\chi} + \left(\frac{1}{2} - \eta\right) \\ & \left[2\alpha\upsilon H^2\psi_{\eta\chi} - \upsilon H^2\psi_\eta + \upsilon H'\psi_\eta + \left(\frac{1}{2} - \eta\right)\upsilon H^2\psi_{\eta\eta}\right] \\ & + \frac{\upsilon}{4h^2}\psi_{\eta\eta} \end{aligned} \tag{8}$$

where $H = \frac{h_x}{h}, H' = \frac{\partial H}{\partial x}$, and $h_x = \frac{\partial h}{\partial x}$. When λ is large, then $\delta = \frac{2\pi a}{\lambda}$ will be a small quantity and similarly $\delta^2 \to 0$. In view of these approximations, some of the factors will become negligibly small i.e. $H' \to 0, H^2 \to 0$. Moreover, it is also assumed that α is of small order. All these assertions are invoked into Eq. (8) and finally we get a most suitable candidate for the vorticity function:

$$\xi_1 = -\frac{\upsilon}{4h^2}\psi_{\eta\eta}. \tag{9}$$

In view of the above definition for the vorticity function, Eq. (7) is reduced to the following form:

$$\begin{aligned} & -\frac{\upsilon h_t}{2h^3}\psi_{\eta\eta} + \frac{\upsilon h_t}{4h^3}\left(\frac{1}{2} - \eta\right)\psi_{\eta\eta\eta} + \frac{\upsilon}{4h^2}\beta'(t)\psi_{\eta\eta\chi} \\ & - \frac{\upsilon}{4h^2}\psi_{\eta\eta t} - \frac{H\upsilon^2}{4h^3}\psi_\eta\psi_{\eta\eta} - \frac{H\upsilon c}{2h^2}\psi_{\eta\eta} \\ & + \frac{H\upsilon c}{4h^2}\left(\frac{1}{2} - \eta\right)\psi_{\eta\eta\eta} = \frac{\upsilon^2}{16h^4}\psi_{\eta\eta\eta\eta} \end{aligned} \tag{10}$$

The problem is further simplified by considering ε, a pseudo variable and assume that ψ is a function of ε instead of t that is, $\psi = \psi(\eta,\varepsilon)$ where ε is wall deformation

(contraction if negative) ratio see [14]. Finally, the simplified version of Eq. (10) is presented over here as:

$$\psi_{\eta\eta\eta\eta}+\frac{8chh_x}{\upsilon}\psi_{\eta\eta}-\frac{8hh_t}{\upsilon}\psi_{\eta\eta}-\frac{4hh_t}{\upsilon}\left(\frac{1}{2}-\eta\right)\psi_{\eta\eta\eta}+4h_x\psi_\eta\psi_{\eta\eta}-\frac{4chh_x}{\upsilon}\left(\frac{1}{2}-\eta\right)\psi_{\eta\eta\eta}=0 \tag{11}$$

The coefficient $\frac{hh_t}{\nu}$ in Eq. (11) is simplified as:

$$\frac{4hh_t}{\nu}=4\varepsilon-4\,\mathrm{Re}\,\delta+4\varphi\delta\varepsilon(x-ct)'$$

where $\varepsilon=\frac{a\dot{a}}{\upsilon}$ is deformation (contraction/expansion) ratio which produces $a(t)=a_0\left(1+\frac{2\upsilon\varepsilon t}{a_0^2}\right)^{\frac{1}{2}}$. The other dimensionless parameters are the wave number $\left(\delta=\frac{2\pi a}{\lambda}\right)$, the Reynolds number $\left(Re=\frac{ca}{\nu}\right)$, amplitude ratio $\left(\varphi=\frac{b}{a}\right)$ and the dimensional channel half spacing (a_0) is defined at $t=0$, $x=0$. It is assumed that the deformation ratio (a) and wave number (δ) are mall parameters, therefore, the product term $\delta\varepsilon$ will also be a smaller quantity .

We set $\alpha_1=\frac{4hh_t}{\upsilon}=4\varepsilon-4\,\mathrm{Re}\,\delta$, $\alpha_2=2h_x=2\delta\varphi$, $\alpha_3=\frac{4Hh^2c}{\upsilon}=4\,Re\delta\varphi$. In view of above definitions for the parameter, Eq. (11) becomes:

$$\psi_{\eta\eta\eta\eta}+2s\psi_{\eta\eta}-s\left(\frac{1}{2}-\eta\right)\psi_{\eta\eta\eta}+Re\psi_\eta\psi_{\eta\eta}=0, \tag{12}$$

where $s=\alpha_1+\alpha_3=4\varepsilon$ and $Re=2\alpha_2=4\,\delta\varphi$. The boundary conditions taken in [17] are used and reduced for the current problem as:

$$\begin{aligned}&\text{at } y=0,\eta=\frac{1}{2}\ :\ \psi=0,\frac{d^2\psi}{d\eta^2}=0,\\&\text{at } y=h,\eta=1\ :\ \psi=F,\frac{d\psi}{d\eta}=-1.\end{aligned} \tag{13}$$

In Eq. (13), F is related to non-dimensional mean flow rate (Q) and $Q=F+1$where F is defined as:

$$F=\int_{\frac{1}{2}}^{1}\left(\psi_\eta+c\right)d\eta=\psi(1)+ch. \tag{14}$$

3 Perturbation solution of the problem

The perturbation solution of Eqs. (12) and (13) is attempted and considered that the Reynolds number (Re) and the deformation ratio (s) are small parameters. The unknown function (ψ) in Eqs. (12) and (13) is expanded in term of Re (a small quantity) and decomposed into more unknown functions, whereas F is also expanded in term of small Re as:

$$\psi=\psi_0+Re\psi_1+O\left(Re^2\right) \tag{15}$$

$$F=F_0+ReF_1+O\left(Re^2\right) \tag{16}$$

Upon substituting the assumed solutions (15)–(16) into Eqs. (12), (13), we get the following differential systems:

3.1 Zeroth-order system

$$\frac{d^4\psi_0}{d\eta^4}=-2s\frac{d^2\psi_0}{d\eta^2}+s\left(\frac{1}{2}-\eta\right)\frac{d^3\psi_0}{d\eta^3}, \tag{17}$$

subject to the boundary conditions:

$$\begin{aligned}&\text{at } \eta=\tfrac{1}{2},\ \psi_0=0,\ \ \tfrac{d^2\psi_0}{d\eta^2}=0,\\&\text{at } \eta=1,\ \psi_0=F_0,\ \tfrac{d\psi_0}{d\eta}=-1.\end{aligned} \tag{18}$$

3.2 First-order system

$$\frac{d^4\psi_1}{d\eta^4}=-2s\frac{d^2\psi_1}{d\eta^2}+s\left(\frac{1}{2}-\eta\right)\frac{d^3\psi_1}{d\eta^3}-\frac{d\psi_0}{d\eta}\frac{d^2\psi_0}{d\eta^2}, \tag{19}$$

with the following associated boundary conditions:

$$\begin{aligned}&\text{at}\eta=\tfrac{1}{2},\ \psi_1=0,\ \ \tfrac{d^2\psi_1}{d\eta^2}=0,\\&\text{at}\eta=1,\ \psi_1=F_1,\ \tfrac{d\psi_1}{d\eta}=0.\end{aligned} \tag{20}$$

For slowly expanding or contracting walls, i.e. small deformation rate $\varepsilon=4s$, it is appeared a small quantity in biomechanics. Therefore, we can express ψ_0 as:

$$\psi_0=\psi_{00}+s\psi_{01}+O\left(s^2\right), \tag{21}$$

$$F_0=F_{00}+sF_{11}+O\left(s^2\right). \tag{22}$$

Substituting the above equations for ψ_0 and F_0 into Eqs. (17), (18) and compare the coefficients of s_0 and s, we get:

$$\frac{d^4\psi_{00}}{d\eta^4}=0, \tag{23}$$

subject to the boundary conditions:

$$\begin{aligned}&\eta=\tfrac{1}{2},\ \psi_{00}=0,\ \ \tfrac{d^2\psi_{00}}{d\eta^2}=0,\\&\eta=1,\ \psi_{00}=F_{00},\ \tfrac{d\psi_{00}}{d\eta}=-1.\end{aligned} \tag{24}$$

and

$$\frac{d^4\psi_{01}}{d\eta^4}=-2\frac{d^2\psi_{00}}{d\eta^2}+\left(\frac{1}{2}-\eta\right)\frac{d^3\psi_{00}}{d\eta^3}, \tag{25}$$

subject to the boundary conditions:

$$\eta = \tfrac{1}{2},\ \psi_{01} = 0,\quad \tfrac{d^2\psi_{01}}{d\eta^2} = 0,$$
$$\eta = 1,\ \psi_{01} = F_{01},\ \tfrac{d\psi_{01}}{d\eta} = 0. \tag{26}$$

In the next few steps we have been evaluated the other unknown terms of ψ by adopting the same procedure used for ψ_0 and finally another set of problems (ODE's & Bc's) is formed. The component ψ_1 of ψ is further decomposed and expanded in term of s and the following set of problems is formed:

$$\frac{d^4\psi_{10}}{d\eta^4} = -\frac{d\psi_{00}}{d\eta}\frac{d^2\psi_{00}}{d\eta^2}, \tag{27}$$

satisfying the following boundary conditions:

$$\eta = \tfrac{1}{2},\ \psi_{10} = 0,\quad \tfrac{d^2\psi_{10}}{d\eta^2} = 0,$$
$$\eta = 1,\ \psi_{10} = F_{10},\ \tfrac{d\psi_{10}}{d\eta} = 0. \tag{28}$$

and

$$\frac{d^4\psi_{11}}{d\eta^4} = -2\frac{d^2\psi_{10}}{d\eta^2} + \left(\frac{1}{2} - \eta\right)\frac{d^3\psi_{10}}{d\eta^3} - \frac{d\psi_{00}}{d\eta}\frac{d^2\psi_{10}}{d\eta^2} - \frac{d\psi_{10}}{d\eta}\frac{d^2\psi_{00}}{d\eta^2}, \tag{29}$$

and the boundary conditions are transformed to:

$$\eta = \frac{1}{2}, \psi_{11} = 0, \frac{d^2\psi_{11}}{d\eta^2} = 0, \tag{30}$$

$$\eta = 1, \psi_{11} = F_{11}, \frac{d\psi_{11}}{d\eta} = 0.$$

Solving the system of Eqs. (23)–(25) and using the value of Eq. (21) we get,

$$\psi_{00}(\eta) = -F_{00} - \eta + c_{02}\eta^2 - 2c_{03}\eta^3, \tag{31}$$

$$\psi_{01}(\eta) = c_{10} + c_{11}\eta + c_{12}\eta^2 + c_{13}\eta^3 + c_{14}\eta^4 + c_{15}\eta^5, \tag{32}$$

where

$$c_{02} = 3 + 6F_{00},\quad c_{03} = -2 - 4F_{00},$$
$$c_{10} = \frac{1}{480}\left(-10c_{02} - 15c_{03} - 48F_{01}\right),$$
$$c_{12} = \frac{1}{160}\left(-70c_{02} - 93c_{03} + 960F_{01}\right),$$
$$c_{13} = \frac{1}{240}\left(-110c_{02} + 93c_{03} - 960F_{01}\right),$$
$$c_{14} = \frac{1}{24}\left(-4c_{02} + 3c_{03}\right),\quad c_{15} = \frac{-3c_{03}}{20}.$$

Therefore, Eq. (21) is converted into the following form when Eqs. (31)–(32) are substituted into it.

$$\psi_0(\eta) = -F_{00} - \eta + c_{02}\eta^2 - 2c_{03}\eta^3 + s\left(c_{10} + c_{11}\eta + c_{12}\eta^2 + c_{13}\eta^3 + c_{14}\eta + c_{15}\eta^5\right) \tag{33}$$

The solution of Eqs. (27)–(29) gives,

$$\psi_{10}(\eta) = d_{10} + d_{11}\eta + d_{12}\eta^2 + d_{13}\eta^3 + d_{14}\eta^4 + d_{15}\eta^5 + d_{16}\eta^6 + d_{17}\eta^7, \tag{34}$$

$$\psi_{11}(\eta) = e_{10} + e_{11}\eta + e_{12}\eta^2 + e_{13}\eta^3 + e_{14}\eta^4 + e_{15}\eta^5 + e_{16}\eta^6 + e_{17}\eta^7 + e_{18}\eta^8 + e_{19}\eta^9, \tag{35}$$

where

$$d_{10} = \frac{1}{13440}\left(140c_{02} - 140c_{02}^2 + 210c_{03} - 336c_{02}c_{03} - 189c_{03}^2 - 13440F_{01}\right),$$

$$d_{11} = \frac{1}{13440}\left(-1120c_{02} + 1120c_{02}^2 - 1680c_{03} + 277c_{02}c_{03} + 1638c_{03}^2\right),$$

$$d_{12} = \frac{1}{13440}\left(2940c_{02} - 2716c_{02}^2 + 4074c_{03} - 6552c_{02}c_{03} - 3861c_{03}^2 + 80640F_{10}\right),$$

$$d_{13} = \frac{1}{13440}\left(-3080c_{02} - 2184c_{02}^2 - 3276c_{03} + 4788c_{02}c_{03} + 2700c_{03}^2 - 53760F_{10}\right),$$

$$d_{14} = \frac{1120c_{02}}{13440},\quad d_{15} = \frac{1}{13440}\left(-448c_{02}^2 + 672c_{03}\right),$$
$$d_{16} = \frac{-672c_{02}c_{03}}{13440},\quad d_{17} = \frac{-288c_{03}^2}{13440},$$

and

$$e_{10} = \frac{1}{215040}\{2240c_{12} + 3360c_{13} - 672c_{03}(5c_{11} + 8c_{12} + 9c_{13}) + 3584c_{14} - 5940c_{03}c_{14} - 448c_{02}(5c_{11} + 2(5c_{12} + 6(c_{13} + c_{14}))) + 3360c_{15} - 75(66c_{02} + 3c_{03})c_{15} - 2(2240d_{12} + 3360d_{13} + 3808d_{14} + 5(784d_{15} + 774d_{16} + 749d_{17} + 21504F_{11}))\},$$

$$e_{11} = \frac{1}{13440}\{28c_{02}(40c_{11} + 80c_{12} + 99c_{13} + 104c_{14}) + 12c_{03}(140c_{11} + 3(77c_{12} + 91c_{13} + 95c_{14})) + 75(38c_{02} + 45c_{03})c_{15} - 4(280c_{12} + 420c_{13} + 462c_{14} + 455c_{15} - 4(140d_{12} + 210d_{16} + 252d_{14} + 280d_{15} + 300d_{16} + 315d_{17}))\},$$

$$e_{12} = \frac{1}{215040}\{-3c_{03}(21728c_{11} + 34944c_{12} + 41184c_{13} + 43340c_{14} + 43325c_{15}) - 2c_{02}(23520c_{11} + 64(679c_{12} + 819c_{13} + 858c_{14}) + 54175c_{15}) + 2(23520c_{12} + 32592c_{13} + 34944c_{14} + 34320c_{15} - 47040d_{12} - 62496d_{13} - 74592d_{14} - 84240d_{15} - 92070d_{16} - 98525d_{17} + 645120F_{11})\},$$

$$e_{13} = c_{02}\left(\frac{11c_{11}}{48} + \frac{13c_{12}}{40} + \frac{57c_{13}}{160} + \frac{5c_{14}}{14} + \frac{1235c_{15}}{3584}\right) + \frac{3c_{03}}{322560}\{36(728c_{11} + 1064c_{12} + 1200c_{13} + 1235c_{14}) + 43925c_{15}\} - 96\{770c_{12} + 819c_{13} + 798c_{14} + 750c_{15} - 14(110d_{12} + 93d_{13} + 111d_{14}) - 1755d_{15}\} + 184140d_{16} + 197050d_{17} - 4F_{11},$$

$$e_{14} = \frac{1}{24}(-2c_{02}c_{11} + 2c_{12} - 4d_{12} + 3c_{13}),$$

$$e_{15} = \frac{1}{60}(-3c_{03}c_{11} - 4c_{02}c_{12} - 3c_{13} - 9d_{13} + 6d_{14}),$$

$$e_{16} = \frac{1}{60}(-3c_{03}c_{12} - 3c_{02}c_{13} - 2c_{14} - 8d_{24} + 5d_{25}),$$

$$e_{17} = \frac{1}{210}\{-9c_{03}c_{13} - 8c_{02}c_{14} + 5(c_{15} - 5d_{15} + 3d_{16})\},$$

$$e_{18} = \frac{1}{336}\{-2(6c_{03}c_{14} + 5c_{02}c_{15} + 18d_{16}) + 21d_{17}\},$$

$$e_{19} = \frac{1}{504}(-15c_{03}c_{15} - 49c_{27}).$$

So that,

$$\psi_1(\eta) = \psi_{10}(\eta) + s\psi_{11}(\eta)$$

$$\Rightarrow \psi_1(\eta) = d_{10} + d_{11}\eta + d_{12}\eta^2 + d_{13}\eta^3 + d_{14}\eta^4 + d_{15}\eta^4 + d_{16}\eta^6 + d_{17}\eta^7 + s\{e_{10} + e_{11}\eta + e_{12}\eta^2 + e_{13}\eta^3 + e_{14}\eta^4 + e_{15}\eta^5 + e_{16}\eta^6 + e_{17}\eta^7 + e_{18}\eta^8 + e_{19}\eta^9)\} \quad (36)$$

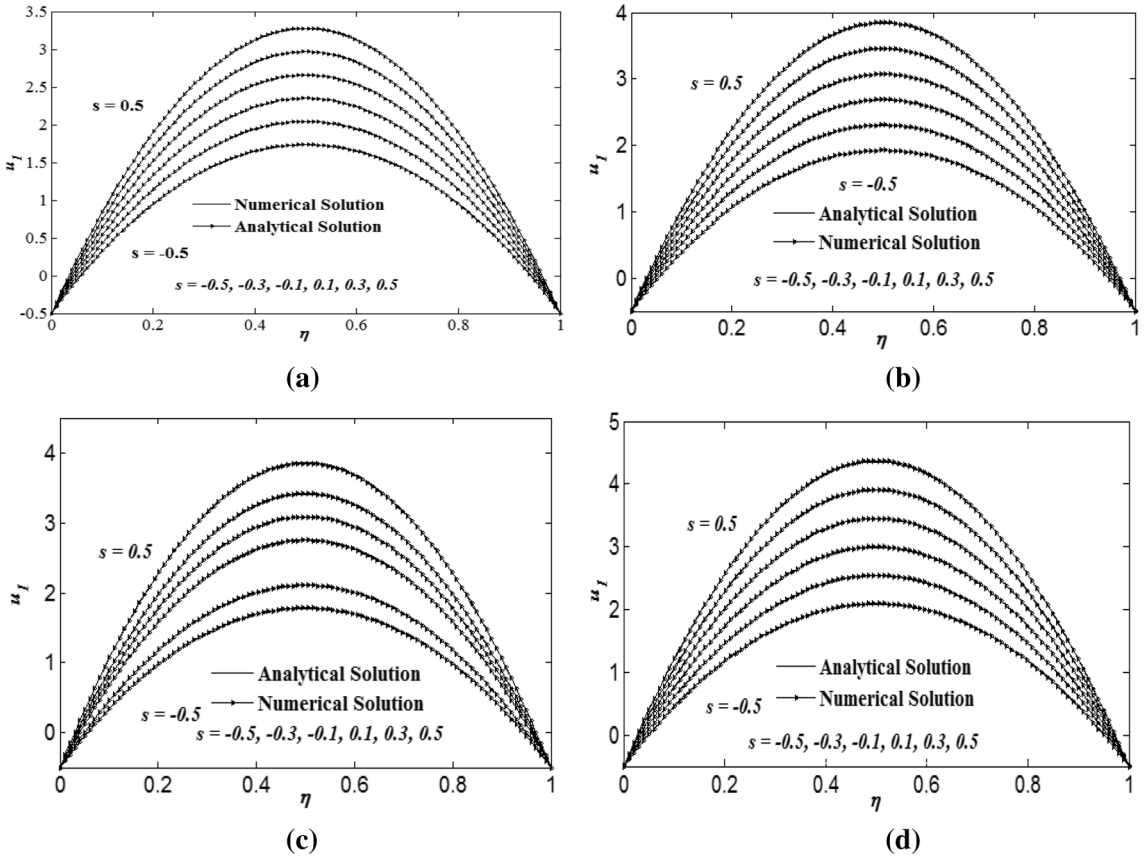

Fig. 2 The axial velocity u_1 is graphed for different s and **a** $Re = 0.0025$, **b** $Re = 0.0625$, **c** $Re = 0.25$ and **d** $Re = 0.475$

Table 1 The two solutions are presented for $\boldsymbol{u}_1$ at $\eta = 0.4949$, when $\boldsymbol{s} = 0.1$ and 0.5

Re	Numerical solution		Perturbation solution		Percent error	
	$s = 0.1$	$s = 0.5$	$s = 0.1$	$s = 0.5$	$s = 0.1$	$s = 0.5$
0.0025	2.6578	3.2789	2.65759	3.27406	0.00790	0.147829
0.0625	2.7580	3.4166	2.75768	3.41110	0.01160	0.161238
0.2500	3.0724	3.8489	3.07045	3.83937	0.06351	0.248218
0.4750	3.4526	4.3730	3.44577	4.35329	0.19821	0.452761
0.5000	3.4951	4.4316	3.48748	4.41040	0.21855	0.480682

Table 2 The two solutions are presented for u_1 at $\eta = 0.4949$ when $s = -0.1$ and -0.5

Re	Numerical solution		Perturbation solution		Percent error	
	$s = -0.1$	$s = -0.5$	$s = -0.1$	$s = -0.5$	$s = -0.1$	$s = -0.5$
0.0025	2.3496	1.7377	2.34936	1.73289	0.010216	0.277571
0.0625	2.4312	1.7828	2.43096	1.77754	0.009872	0.295915
0.2500	2.6874	1.9240	2.68599	1.91706	0.052495	0.362013
0.4750	2.9969	2.0942	2.99201	2.08449	0.163435	0.465821
0.5000	3.0314	2.1131	3.02602	2.10310	0.177791	0.475488

Hence,

$$\begin{aligned}\psi(\eta) = &-F_{00} - \eta + c_{02}\eta^2 + 2c_{03}\eta^3 + s\left(c_{10} + c_{11}\eta + c_{12}\eta^2 + c_{13}\eta^3 + c_{14}\eta^4 + c_{15}\eta^5\right)\\ &+ \mathrm{Re}\left\{d_{10} + d_{11}\eta + d_{12}\eta^2 + d_{13}\eta^3 + d_{14}\eta^4 + d_{15}\eta^5 + d_{16}\eta^6 + d_{17}\eta^7\right.\\ &+ s\left(e_{10} + e_{11}\eta + e_{12}\eta^2 + e_{13}\eta^3 + e_{14}\eta^4 + e_{15}\eta^5 + e_{16}\eta^6 + e_{17}\eta^7\right.\\ &\left.\left.+e_{18}\eta^8 + e_{19}\eta^9\right)\right\}\end{aligned} \tag{37}$$

4 Results

The governing equation are reduced into a simplest ODE with the help of useful transformations and established approximations. The final problem contains several dimensionless parameters and perturbation method is used for the solution of this problem for small value of the parameters involved in the problem. Moreover, a numerical solution of final problem is also formed. Effects of all the parameters i.e. surface deformation and peristaltic motion are seen on the flow characteristics and field quantities. Response of the main flow to the different parameters s and Re is also noted in different graphs. Both the velocity components, pressure, pressure rise (drop) per volume flow rate, and shear stress profiles are presented in different figures. A set of different results against different parameters is formed and the new observations are presented in graphs and tables.

Besides that the two different solutions for each of these quantities are compared in different tables and excellent results are found.

4.1 Axial velocity

The axial velocity is graphed in Fig. 2 and this figure has four subplots. Effects of the parameter s are seen on axial velocity for positive Re. The two different solutions for the velocity component are also compared in this figure. The two solutions are exactly matched for wide range of parameter values and these assertion are reflected in Fig. 2. The variation in axial velocity profiles are noted for different s and the deformation rate is changed from positive to negative and fixed Re. It is confirmed that the two solutions are exactly matched for this range of s whereas the error in analytical solution is negligibly small. The perturbation and numerical solutions are compared in Tables 1, 2 and these solutions are found at different points about the mid line of channel. The positive (negative) values of s are representing the walls expansion (contraction) ratio. The similar and symmetrical graphs in Fig. 2 are decreased with the decreasing of s. In Table 1, the axial velocity component (u_1) is calculated about the mid of the channel for $s > 0$ and different Re. In Table 2, the perturbation and numerical solutions are matched for $s < 0$ and different Re. The differences between the two solutions are very small in the limiting values of governing parameters. It is observed that the error is minimum for fixed value 0.5 of the constants c, h, F_{00}, F_{01}, F_{10}, and F_{11}, Re has values in the interval $0 \le Re \le 0.5$ and wall expansion (contraction) s has small values. Note that the solution strictly varies with F and s small variation in F gives rise to significant changes in error between the two solutions. Any small changes in s and Re creates variation in F. For manipulated choices of s, Re and different parts of F, it is suggested that F must be unity or smaller in order to produce more accurate results. In view of these restrictions, the analytical solution provides good results for bit larger values of the perturbation parameters involved in the problem.

4.2 Normal velocity

Profiles of normal velocity are graphed in Fig. 3 and consequences of different parameters are seen on it. The figures are plotted for different s and Re and anti-symmetric profiles of the normal velocity are increased with decreasing of s where s lies in the interval $-0.5 \le s \le 0.5$. Note that the normal velocity vanishes at the midway of the channel i.e. $\eta = 0.5$, therefore, the flow properties are calculated at the mid points of center line and upper plate. For all such points, the two solutions are also compared to each other. In Tables 3, 4, the analytical solutions are compared with numerical solutions for small values of s and different Re. However, it is noted that the differences between results are negligibly small when $0 \le Re \le 0.8$ and $|s| \le 0.5$. The two solutions are also graphed in Fig. 3 which are exactly overlapped. Moreover, the two solutions for this velocity component are exactly same and the results are shown in the respective figures.

4.3 Pressure distributions is compared with classical model

The profiles of pressure distribution are plotted against η for different s & Re. Note that we found a mathematical relation for both normal and axial pressure gradients. It is obtained by putting the expressions for u_1 and v_1 from Eq. (6) into Eq. (3) and get the following results.

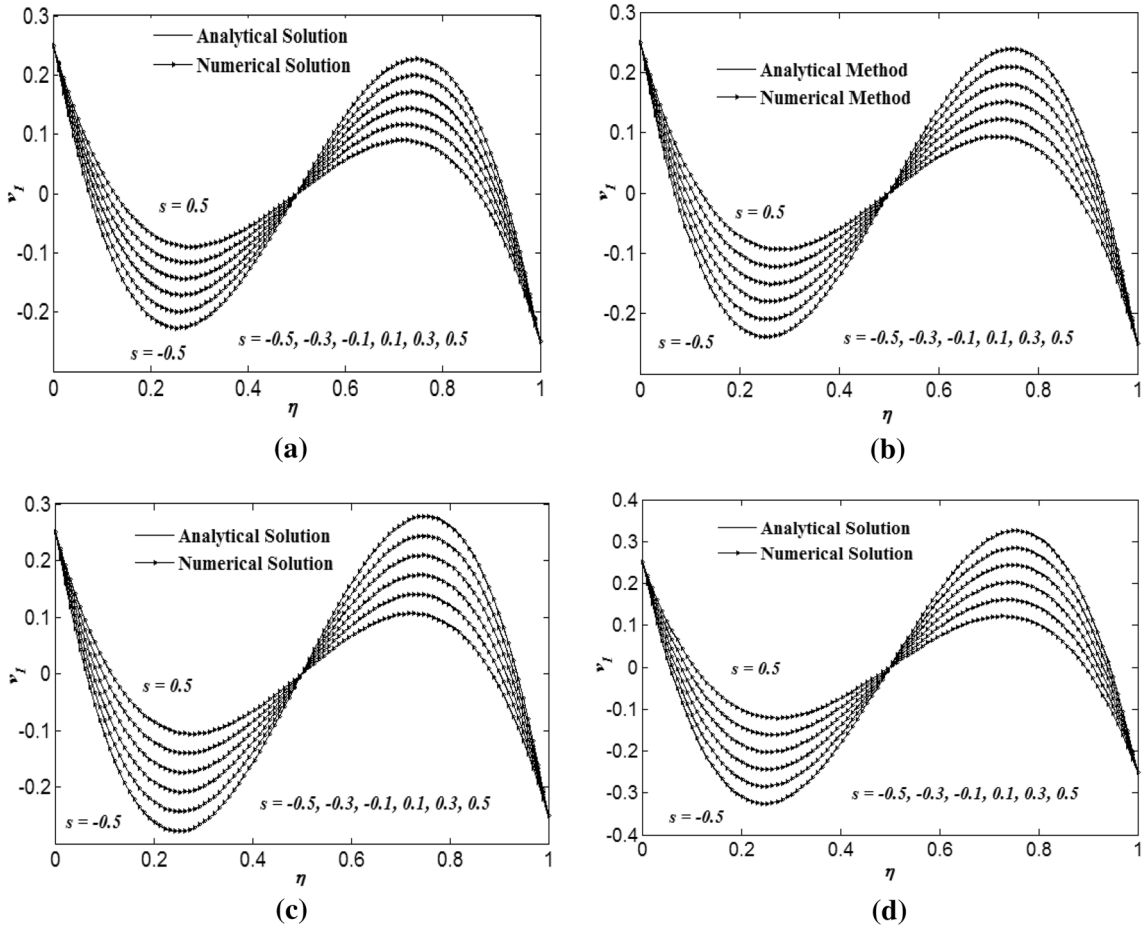

Fig. 3 The normal velocity v_1 is graphed for different s when **a** $Re = 0.0025$, **b** $Re = 0.0625$, **c** $Re = 0.25$, **d** $Re = 0.475$

Table 3 The two solutions are shown for v_1 at $\eta = 0.2424$ when $s = 0.1$ and 0.5

Re	Numerical solution		Perturbation solution		Percent error	
	$s = 0.1$	$s = 0.5$	$s = 0.1$	$s = 0.5$	$s = 0.1$	$s = 0.5$
0.0025	−0.1695	−0.2258	−0.169502	−0.225945	0.00118	0.05867
0.0625	−0.1788	−0.2385	−0.178824	−0.238640	0.01342	0.11103
0.2500	−0.2079	−0.2780	−0.207956	−0.278309	0.02693	0.11103
0.4750	−0.2427	−0.3252	−0.242915	−0.325913	0.08851	0.21877
0.5000	−0.2465	−0.3304	−0.246799	−0.331202	0.12115	0.24215

Table 4 The two solutions are shown for v_1 at $\eta = 0.2424$ when $s = -0.1$ and -0.5

Re	Numerical solution		Perturbation solution		Percent error	
	$s = -0.1$	$s = -0.5$	$s = -0.1$	$s = -0.5$	$s = -0.1$	$s = -0.5$
0.0025	−0.1413	−0.0847	−0.141280	−0.0848361	0.014156	0.016043
0.0625	−0.1489	−0.0889	−0.148916	−0.0891006	0.010744	0.225139
0.2500	−0.1727	−0.1022	−0.172780	−0.1024270	0.046302	0.221621
0.4750	−0.2012	−0.1181	−0.201416	−0.1184190	0.107241	0.269382
0.5000	−0.2044	−0.1199	−0.204598	−0.1201960	0.096775	0.246264

$$\frac{1}{\rho}\frac{\partial p}{\partial x} = \frac{\upsilon^2}{8h^3}\psi_{\eta\eta\eta} + \frac{\upsilon h_t}{2h^2}\psi_\eta - \frac{\upsilon h_t}{2h^2}\left(\frac{1}{2}-\eta\right)\psi_{\eta\eta} + \frac{H\upsilon^2}{4h^2}\psi_\eta^2 + \frac{H\upsilon c}{2h}\psi_\eta - \frac{H\upsilon c}{2h}\left(\frac{1}{2}-\eta\right)\psi_{\eta\eta} \quad (38)$$

The non-dimensionalized axial pressure gradient is defined bellow and normalized with $\frac{h^3}{\upsilon^2}$.

$$\frac{h^3}{\upsilon\mu}\frac{\partial p}{\partial x} = \frac{1}{8}\psi_{\eta\eta\eta} + \frac{s}{8}\psi_\eta - \frac{s}{8}\left(\frac{1}{2}-\eta\right)\psi_{\eta\eta} + \frac{Re}{16}\psi_\eta^2 \quad (39)$$

The appropriate definition for pressure rise per wavelength is:

$$\Delta p_\lambda = \int_0^{2\pi} \frac{dp}{dx}dx. \quad (40)$$

The pressure rise per wavelength (Δp_λ) is computed by substituting the above approximations of the series form i.e. $F0 = F_{00} + sF_{01}$ and $F1 = F_{10} + sF_{11}$. By inserting the approximated relations, the pressure rise per wavelength is equipped with new quantities and the profiles are graphed against volume flow rate (Q) in Fig. 4. Note that the pressure rise per wavelength increases with the increase of s. The profiles are changed linearly with Q and these observations are confirmed from [17].

On the other hand Eq. (4) is used for evaluation of normal pressure gradient. The expressions for u_1 and v_1 are substituted into Eq. (6). Later on, ψ is used from Eq. (37) and a standard relation is obtained for the pressure gradient.

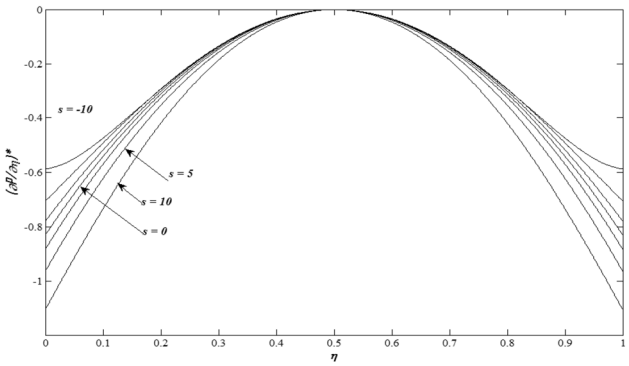

Fig. 5 Normal pressure gradient is graphed for different s

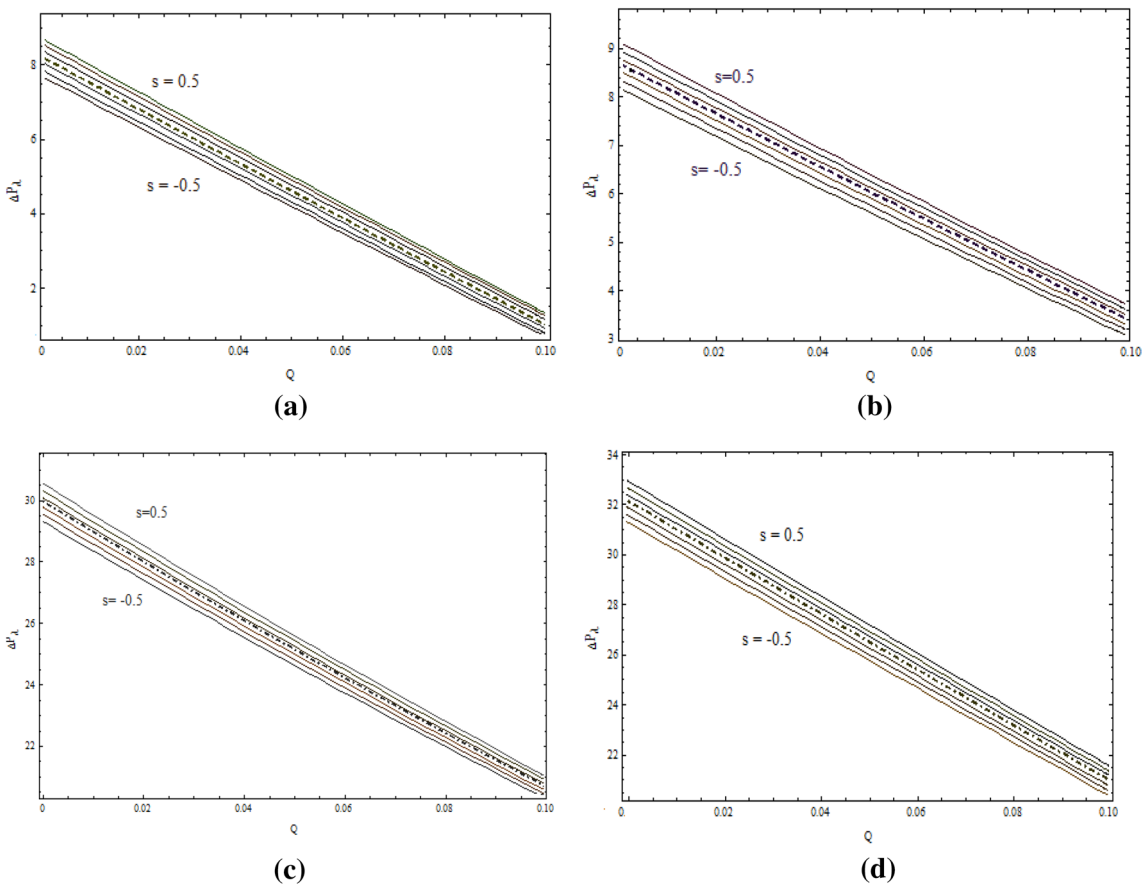

Fig. 4 The graphs of pressure rise per wavelength against Q are shown (*a*) $Re = 9.0$, $F1 = 0.3$, (*b*) $Re = 12.72$, $F1 = 0.025$, **c** $Re = 12.72$, $F1 = 0$, **d** $Re = 12.6$, $F1 = 0.25$ and matched with [17]

Table 5 The two solutions are shown for $\left(\frac{\partial p_n}{\partial \eta}\right)^* = \frac{h^2}{Re\rho\upsilon^2}\left(\frac{\partial p_n}{\partial \eta}\right)$

η	Numerical solution		Perturbation solution		Percent error	
	$s=0.1$	$s=0.5$	$s=0.1$	$s=0.5$	$s=0.1$	$s=0.5$
0.0100	−0.8020	−0.8118	−0.779433	−0.802667	2.81385	1.12504
0.0240	−0.7584	−0.7673	−0.741064	−0.760378	2.2659	0.9022
0.4760	−0.0021	−0.0021	−0.002310	−0.002190	10	4.2858
0.5240	−0.0021	−0.0021	−0.002310	−0.002190	10	4.2858
0.9760	−0.7584	−0.7673	−0.741064	−0.760378	2.2859	0.9022

$$\frac{h^2}{\rho\upsilon^2}\frac{\partial p_n}{\partial \eta} = -\frac{sRe}{8}\left(\frac{1}{2}-\eta\right)\psi_\eta + \frac{sRe}{8}\left(\frac{1}{2}-\eta\right)^2\psi_{\eta\eta} + \frac{Re}{8}\psi_{\eta\eta} - \frac{Re}{8}\left(\frac{1}{2}-\eta\right)\psi_{\eta\eta\eta}. \tag{41}$$

Remember that Eq. (4) is used for the solution of normal pressure distribution. Later on it is integrated between 1/2 and η and used the boundary conditions given in Eq. (13). However, Eq. (41) gives the non-dimensionalized form of normal pressure gradient and it is scaled by Re. It is graphed in Fig. 5 for different s. The normal pressure drop vanishes at the midway of the channel for small s. In Table 5, solutions for $\left(\frac{\partial p_n}{\partial \eta}\right)^* = \frac{h^2}{Re\rho\upsilon^2}\left(\frac{\partial p_n}{\partial \eta}\right)$ are compared. It is confirmed that the normal pressure gradient decreases with increase of s for $|s| < 10$.

5 Wall shear stress

We used Newton's law of viscosity for evaluation of shear stress. Effects of s and Re are calculated on shear stress: The law has the following well-known mathematical form:

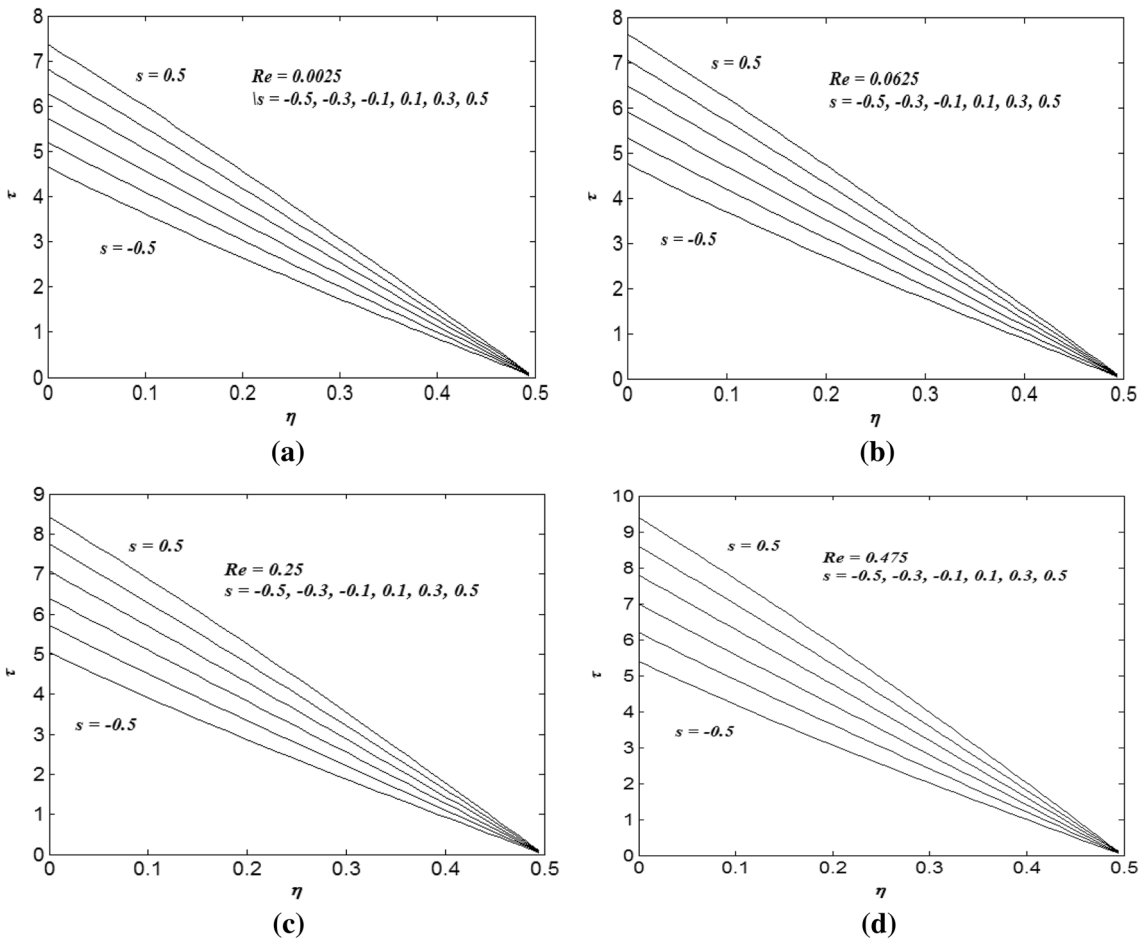

Fig. 6 The shear stress profiles are graphed against η for different s and **a** $Re=0.0025$, **b** $Re=0.0625$, **c** $Re=0.25$ and **d** $Re=0.475$

Table 6 The two solutions are shown for shear stresses when η=0.2525, s=0.3, −0.3

Re	Numerical solution		Perturbation solution		Percent error	
	s=0.3	*s*=−0.3	*s*=0.3	*s*=−0.3	*s*=0.3	*s*=−0.3
0.0025	3.4658	2.4934	3.46008	2.48758	0.165314	0.233962
0.0625	3.5879	2.5567	3.58118	2.55030	0.187648	0.250951
0.2500	3.9749	2.7567	3.95962	2.74629	0.385896	0.379057
0.4750	4.4528	3.0011	4.41374	2.98148	0.884960	0.658062

$$\tilde{\tau} = \mu\left(\frac{\partial u_1}{\partial y} + \frac{\partial v_1}{\partial x}\right). \tag{42}$$

The shear stress in the above equation is evaluated by putting the expressions for u_1 and v_1. The values of velocity components are noted in Eq. (6) and substituted into Eq. (42) and we get:

$$\tilde{\tau} = \beta_4 \psi_{\eta\eta}. \tag{43}$$

where $\beta_4 = \frac{\mu v}{4h^2}$. In dimensionless sense, we have,

$$\tau = \frac{\tilde{\tau}}{\beta_4} = \psi_{\eta\eta}. \tag{44}$$

Effects of different parameters are illustrated on the characteristics of the shear stress profiles in Fig. 6. For different *s* and fixed *Re*, the profiles are approaching zero at the center line. It is noted that it is increasing with the increase of *s* for $-0.5 \le s \le 0.5$. The shear stresses is also increased with the increase of *Re* and it is changed linearly with η. The two solutions for τ are matched in Table 6 for different values of *Re* and *s*=0.3. Only those numerical values of τ are considered for which the error between the two solutions is of significant order. The numerical and analytical solutions are matched for *s*=−0.3 and different *Re*.

6 Conclusion

Viscous fluid flow in deformable and peristaltically moving walls in studied and different flows field properties are examined for small values of deformation rate and wave number. Set of variable is defined in such a way that the governing partial differential equation are transformed into a single ODE's with boundary conditions. New variables are formed and used for the simplification of the equation of motion. Well-established approximations and assumption are used for further simplification of modeled equations. These simplification procedures helped us to simplify the governing PDE's and converted them into a boundary value ODE, which is simplest one and easy to solve. The joint effects of physical parameters i.e. Reynolds number (*Re*) and deformation ratio (*s*) of the channel have been observed on the flow quantities. All results in the current analysis give rise to considerable influence on flow-field characters. Abrupt changes in pressure rise against volume flow rate (*Q*) are noted for large *Re* and profiles of [17] are also recovered. The solution of the last ODE is attempted by two methods. The two different solution are matched in different figures and tables and the two solution are same for small value of *Re* and *s*. The problem of peristaltic flow in a channel of deformable walls is formulated in a convenient form with the help of established mathematical simulations and gives the bench mark solutions. Moreover, effects of peristalsis and deformation are analyzed independently and jointly.

Compliance with ethical standards

Conflict of interest The authors declare that they have no conflict of interest.

References

1. Shapir AH (1967) Proceeding workshop on ureteral in Children National Academy of Science Natural Research Council, 109
2. Burns JC, Parkes T (1967) Peristaltic motion. J Fluid Mech 29:731–737
3. Barton C, Raynor S (1968) Peristaltic flow in tubes. Bull Math Biophys 30:663–680
4. Yin FCP, Fung YC (1971) Comparison of theory and experiment in peristaltic transport. J Fluid Mech 47:93–112
5. Tong P, Vawter D (1972) An analysis of peristaltic pumping. J Appl Mech 39:857–862
6. Fung YC, Yih CS (1968) Peristaltic transport. J Appl Mech 35:669–675
7. Shapiro AH, Jaffrin MY, Weinberg SL (1969) Peristaltic pumping with long wavelengths at low Reynolds number. J Fluid Mech 37:799–825
8. Jaffrin MY, Shapiro AH (1971) Peristaltic pumping. Anal Rev Fluids Mech 3:13–36
9. Takabatake S, Ayukawa K (1982) Numerical study of two-dimensional peristaltic flows. J Fluid Mech 122:439–465
10. Srivastava LM, Srivastava VP (1984) Peristaltic transport of blood: Casson model-II. J Biomech 17:821–829

11. Goto M, Uchida S (1990) Unsteady flows in a semi-infinite expanding pipe with injection through wall. Trans Jpn Soc Aeronaut Space Sci 33:14–21
12. Dauenhauer EC, Majdalani J (1999) Unsteady flows in semi-infinite expanding channels with wall injection. AIAA 1999:3523
13. Dauenhauer EC, Majdalani J (2001) Exact self-similarity solution of the NavierStokes equations for a deformable channel with wall suction or injection. AIAA 2001:3588
14. Majdalani J, Chong Z, Christopher AD (2002) Two-dimensional viscous flow between slowly expanding or contracting walls with weak permeability. J Biomech 35:1399–1403
15. Kawamura N, Yamashiki N, Saitoh H, Sahara K (2000) Significance of peristaltic squeezing of sperm bundles in the silkworm, Bombyx mori: elimination of irregular eupyrene sperm nuclei of the triploid. Zygote 9:159–166
16. Matebese BT, Adem AR, Khalique CM, Hayat T (2010) Two-dimensional flow in a deformable channel with porous medium and variable magnetic field. Math Comp App 15:674–784
17. Khan Marwat DN, Asghar S (2011) Peristaltic flow in a deformable channel. Z Naturforsch 66:24–32
18. Akram S, Zafar M, Nadeem S (2018) Peristaltic transport of a Jeffrey fluid with double-diffusive convection in nanofluids in the presence of inclined magnetic field. Int J Geom Methods Mod Phys 15:1850181
19. Sadaf H, Akbar MU, Nadeem S (2018) Induced magnetic field analysis for the peristaltic transport of non-Newtonian nanofluid in an annulus. Math Comput Simulat 148:16–36
20. Shahzadi I, Nadeem S (2019) Consequences of compliant walls for peristaltic transportation in a channel having porous medium and porous boundaries. Can J Phys 97:599–608
21. Saleem S, Al-Qarni MM, Nadeem S, Sandeep N (2018) Convective heat and mass transfer in magneto Jeffrey fluid flow on a rotating cone with heat source and chemical reaction. Commun Theor Phys 70:534
22. Rashid M, Nadeem S (2019) EMHD flow through microchannels with corrugated walls in the presence of nanofluid. Can J Phys 97:701–720
23. Ijaz S, Nadeem S (2018) Transportation of nanoparticles investigation as a drug agent to attenuate the atherosclerotic lesion under the wall properties impact. Chaos Soliton Fract 112:52–65
24. Saleem S, Nadeem S, Rashidi MM, Raju CSK (2018) An optimal analysis of radiated nanomaterial flow with viscous dissipation and heat source. Microsyst Technol 25:683–689
25. Qasim M, Afridi MI, Wakif A, Saleem S (2019) Influence of variable transport properties on nonlinear radioactive jeffrey fluid flow over a disk: utilization of generalized differential quadrature method. Arab J Sci Eng 44(6):5987–5996